

# A Panoramic Stereo Imaging System for Aircraft Guidance

Saul Thurrowgood<sup>1</sup>, Wolfgang Stuerzl<sup>2</sup>, Dean Soccol<sup>1</sup>, Mandyam Srinivasan<sup>1</sup>

<sup>1</sup>Biorobotics Laboratory, Queensland Brain Institute The University of Queensland, Brisbane, Queensland, 4072, and ARC Centre of Excellence in Vision Science, Australia

<sup>2</sup>Computer Science Department VI, Technical University Munich, Boltzmannstr. 3, 85748 Garching, Germany  
[s.thurrowgood@uq.edu.au](mailto:s.thurrowgood@uq.edu.au), [stuerzl@in.tum.de](mailto:stuerzl@in.tum.de), [d.soccol@uq.edu.au](mailto:d.soccol@uq.edu.au), [m.srinivasan@uq.edu.au](mailto:m.srinivasan@uq.edu.au)

near-panoramic vision as well as near-panoramic range range information.

## Abstract

*This paper describes an imaging system for aircraft guidance that provides panoramic stereo vision to facilitate surveillance, obstacle detection and avoidance, terrain following and landing. The system uses a single video camera in conjunction with a set of specially shaped reflective surfaces to enable the detection of objects in the environment and estimation of their range through stereo. The advantage of this device over systems that use optic flow information for visual guidance is that it does not rely on the movement the aircraft. Therefore, it can be used even at low flight speeds or hover.*

## 1. Introduction

There is considerable interest in the design of guidance systems for UAVs that use passive sensing (such as vision), rather than active sensing which can be bulky, expensive and stealth-compromising. A recent trend in biologically inspired vision systems for aircraft guidance has been to exploit optic flow information for collision avoidance, terrain following, gorge following and landing (e.g. [Chahl and Srinivasan, 1999; Barrows *et al.*, 2003; Srinivasan *et al.*, 2004; Ruffier and Franceschini, 2005; Zufferey and Floreano, 2006]). However, the acquisition of optic flow requires that the aircraft be in motion, which makes such systems unviable during periods of low flight speed or hover. On the other hand, the use of stereo vision enables estimation of range regardless of the aircraft's speed, and works even when the aircraft is stationary. Moreover, systems that rely on optic flow for extracting range information need to discount components of optic flow that are induced by rotations of the aircraft, and use only those components of optic flow that are generated by the translational component of motion. The reason is that it is only the translational components of optic flow that provide information on the range to objects in the environment. Vision systems that exploit stereo information do not require this computationally elaborate procedure. Wide-angle stereo systems have previously been designed for aircraft (e.g. [Tisse *et al.*, 2007]). However, they typically use two cameras, which require synchronization and alignment. Furthermore, they usually use conventional fish-eye lenses that rarely cover visual fields greater than a hemisphere. The system presented here uses a single camera, and can potentially deliver

## 2. Design of imaging system

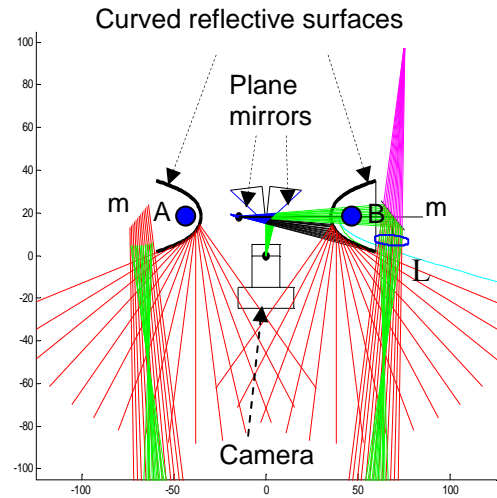


Fig. 1 Schematic illustration of imaging system

The system consists of a single camera that views a pair of curved, horizontally apposed reflecting surfaces via a pair of angled plane mirrors, as shown in Fig. 1. Each of the curved surfaces is designed to capture a near-panoramic view of the environment. Their profiles are designed to achieve constant elevational gain, like the panoramic reflective mirrors described in [Chahl and Srinivasan, 1997]. This angular gain is 12.65. Unlike many other optical systems that have been used for panoramic imaging [Yagi *et al.*, 1996; Nayar, 1997; Hicks and Bajcsy, 2001], the constant-gain design used here ensures that a given angular elevation always subtends a constant number of pixels in the camera, thus making optimum use of the camera's resolution. This design also simplifies the calculation of stereo disparities, as discussed below. The effective viewpoint of each curved reflector is shown by the blue dot (A, B). (The viewpoint is not constant, but wanders by a few mm depending upon the direction of view [Chahl and Srinivasan, 1997].) In effect, the system simulates a pair of human eyes, each with a near-panoramic field of view, and with a stereo baseline (interocular separation) corresponding to the distance between A and B (ca. 80mm). Each of the curved mirrors carries a 7 mm dia. axial aperture, through which a region

in front of the device is viewed stereoscopically via reflection by a pair of auxiliary plane mirrors  $m$ , as shown by the green rays. This facilitates high-resolution viewing and ranging of objects directly in front of the vision system (i.e. behind the camera). A lens  $L$ , associated with each auxiliary mirror, ensures that the camera can be focussed optimally to view the panoramic images as well as the frontal views.

### 3. Realization of imaging system

Fig. 2 shows a realization of the system. Each curved reflector has a base diameter of 33.70 mm and a base-to-tip height of 24.28 mm. The distance between the bases of the reflectors is 120.6 mm. The plane mirrors consist of 45 deg prisms with reflective bases (Edmund Scientific) of dimension 35 mm x 25 mm. An analog CCD camera (640x 480 pixels) with a FOV of 40 deg x 60 deg is used. The camera lens is focussed to a point 6mm below the tip of each reflector, to ensure that most of the

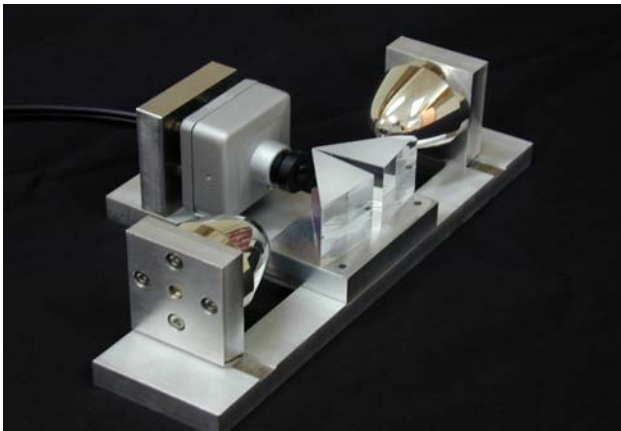


Fig. 2. View of realization of imaging system

image captured by the curved reflectors is in focus. (The position of focus varies by a few mm, depending upon the direction of view [Chahl and Srinivasan, 1997]. The components are mounted rigidly on a purpose-machined aluminium base, but with provision for minor adjustments of alignment. In the current hardware version the auxiliary frontal stereo system has not been implemented, and this feature will not be discussed any further.

The field of view of the system (5.42 steradians mono, 4.05 steradians stereo) is not as large as it can potentially be, because (a) the brackets in the frame to support the whole assembly cause some occlusion of the visual field - they were made relatively large in cross section to ensure rigidity and resistance to impact; and (b) the body of the camera that was used in this initial realization was relatively large, thus occluding some of the visual field. These design shortcomings will be removed in subsequent realizations.

### 4. Loci of constant disparity

If we assume (as an approximation) that the viewpoints of the curved mirrors are fixed at positions A and B (Fig. 1), then, for any plane passing through these points, the locus of constant disparity will lie on a circle in the plane that

passes through A and B, with a radius equal to  $\frac{d}{2\sin\theta}$ ,

where  $d$  is the distance between A and B (the stereo baseline) and  $\theta$  is the angular disparity (Fig. 3). The centre of the circle (C) will be at a perpendicular distance of

$\frac{d}{2\tan\theta}$  from the baseline (Fig. 3).

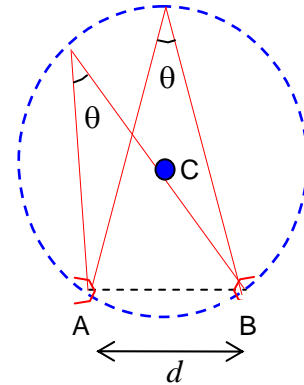


Fig. 3. Locus of constant angular disparity in a plane.

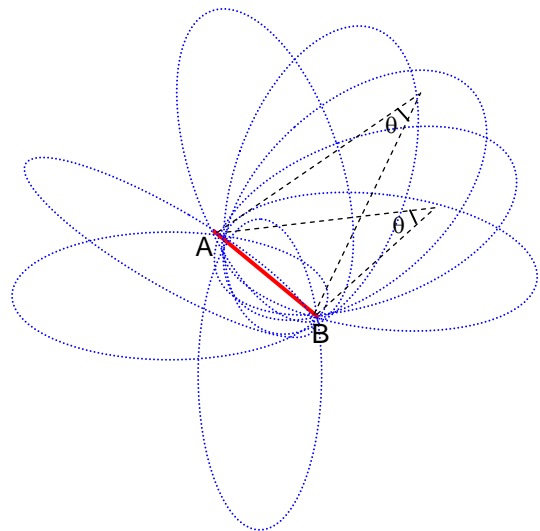


Fig. 4. Surface of constant angular disparity in 3-D.

In three dimensions, the loci of all points that have a given disparity will therefore correspond to the surface of revolution that is generated by rotating the circle about the stereo baseline, as shown in Fig. 4. Thus, surfaces of constant angular disparity will have the shape of a torus

whose ring has a centre radius of  $\frac{d}{2\tan\theta}$ , and a thickness  $\frac{d}{\sin\theta}$ .

## 5. Tests in an indoor laboratory environment

Fig. 5a shows a raw image captured by the camera in an indoor laboratory setting. Figs. 5b and 5c show digitally unwarped versions of the subimages from the left and right mirrors. The unwarping is done by representing the pixel positions in each subimage of the raw image in terms of polar coordinates  $(r, \theta)$  relative to the centre of each subimage, and replotting these as Y and X coordinates, respectively, in cartesian space. Because of the constant angular gain property of the curved mirrors, the Y displacement of a given feature between the two unwarped images is directly proportional to the angular disparity of that feature. This facilitates direct and efficient computation of range.

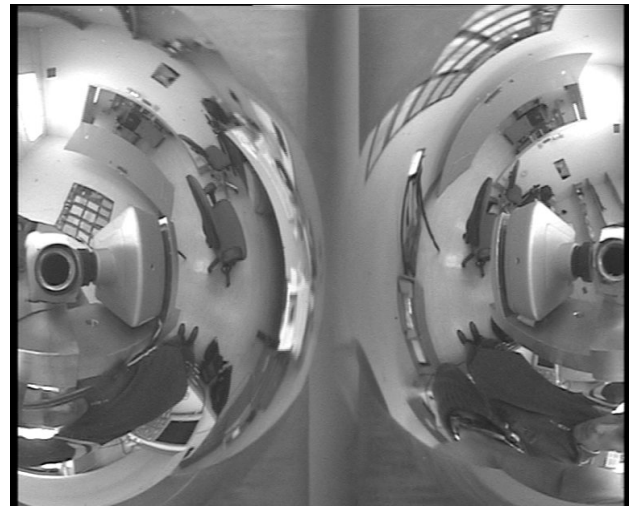
## 6. Offset measurement and compensation

The Y displacement between the two unwarped images represents pixel disparity only if the optics of the system are perfectly aligned, and any systematic offsets are measured and corrected for. Since no alignment can be perfect, the offsets were determined by viewing a distant point source (the moon, which, theoretically, should have zero disparity) and measuring the X and Y offsets between the moon's positions in the unwarped left and right subimages. The offsets were measured for a wide range of viewing directions by mounting the system on a tripod and scanning the night sky during a full moon. Fig. 6a shows one example of the raw images of the moon as captured by the left and right curved mirrors. Fig. 6b shows the positions of the moon in the unwarped subimages. The X and Y offsets, interpolated between sample points, are shown in Fig. 7. These offsets, which are disparities caused by misalignments and lens distortions, should be subtracted out before the true disparity is measured.

Once the offsets have been determined in this way, true disparities can be measured for a 'standard' 3-d environment (e.g. a textured chamber) and this standard environment can be used to re-calibrate the offsets whenever necessary, without any need to rely on the moon again.

## 7. System validation and range calibration

Having determined the offsets, the next step is to calibrate the disparity readings in terms of range. This was done by positioning the device in front of a vertical, visually textured surface and acquiring images at various distances from the surface. The viewing direction was normal to the axes of the two curved surfaces, and was



a



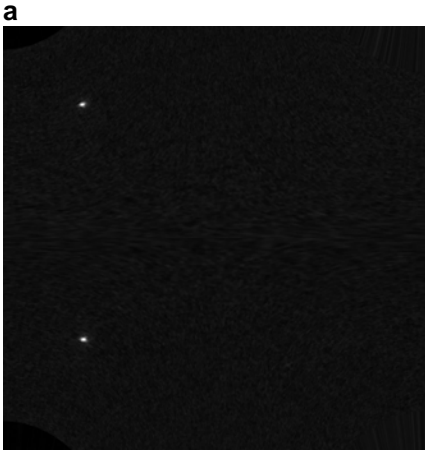
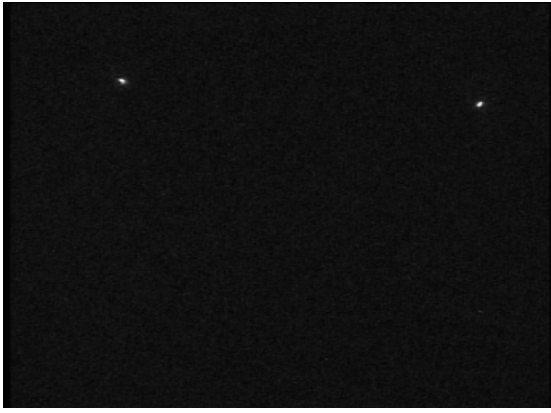
b



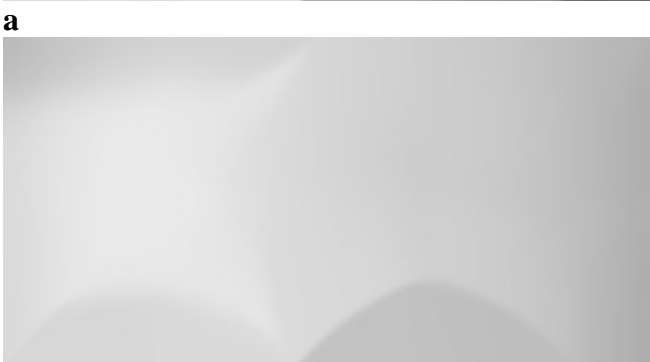
c

Fig. 5 Raw image of an indoor laboratory scene (a), and unwarped versions of subimages from left mirror (a) and right mirror (b).

directly opposite to the camera's optical axis. At each distance, the Y displacement of a frontal 41 x 41 pixel patch was measured between the two images, after the X and Y offsets were removed. This is the true disparity, after accounting for the X and Y offsets. The residual Y displacement was computed using a correlation algorithm



**a**  
**b**  
Fig. 6. Raw images of moon (a) and their positions in the unwarped subimages (b)



**a**  
**b**  
Fig. 7. Results of moon-based offset measurements: Measured X offset (a) and Y offset (b). Scale (Black to white) ranges from -30 to +30 (X) and 10 to 40 (Y).

[Fua, 1993]. The results are shown in Fig. 8. The data are well approximated by a rectangular hyperbola, as would be expected if disparity is inversely proportional to range.

The disparity map computed for the scene of Fig. 5 is shown in Fig. 9. While this computation has not been ground-truthed, it is clear that there is good qualitative agreement with the relative ranges to the various objects in the scene.

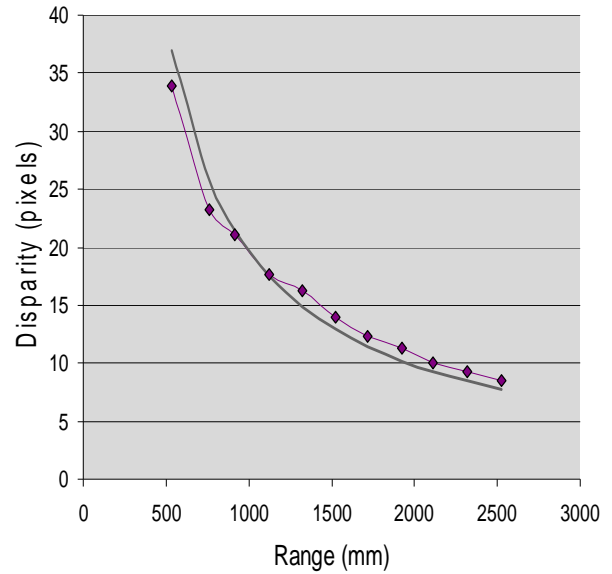


Fig. 8. Range calibration. Diamonds show disparity readings at different ranges. Blue curve shows least squares fit of a rectangular hyperbola:  $\text{Disparity} = 19690/\text{Range}$

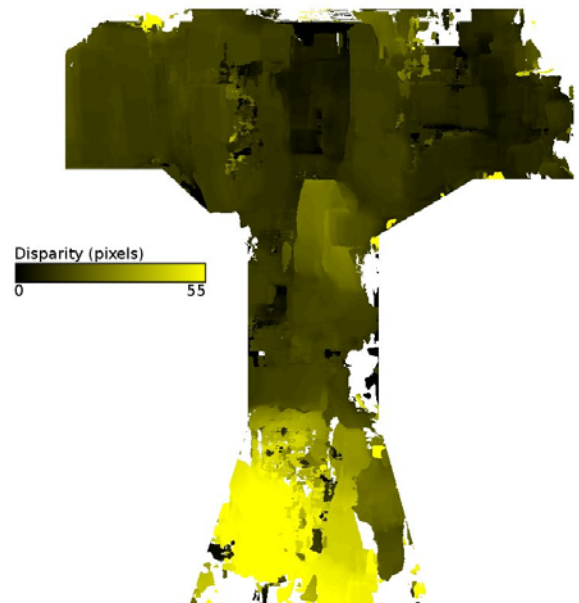


Fig. 9. Disparity map computed for scene of Fig. 5. Disparity is inversely proportional to range.

## 8. Test of system on an aircraft

The system was then tested by mounting it on the underside of a model aircraft (Fig. 10). A raw image taken at low altitude and level flight is shown in Fig. 11. Unwarped versions of this image, and the computed disparity map are shown in Fig. 12. As expected, the disparity of the ground is high everywhere, indicating its proximity. The disparity is highest directly below the aircraft and decreases with more lateral viewing directions, as would be expected with flat horizontal terrain. Fig. 13 shows results from flight at a higher altitude, where the aircraft has a positive pitch attitude and is banking sharply to the right. As expected, the disparities are generally much lower than in the case of Fig. 12, because of the greater altitude, and the ground is much closer toward the rear right-hand portion of the system's visual field, because of the positive pitch and the sharp bank to the right. Thus, the disparity map provides information on the height of the aircraft above the ground, as well as its attitude relative to the ground. The results indicate that the vision system is well suited for use in tasks such as automated terrain following, attitude control and landing.

Repeated offset calibration checks using the moon reveal that the system is quite robust to the vibrations that occur during flight.

A noteworthy additional feature of the vision system is that the wide visual field of the device permits imaging of a substantial portion of the horizon around the aircraft. As the attitude of the aircraft changes, the horizon shifts and distorts in predictable ways that depend upon the magnitude and polarity of the roll and the pitch. This offers the potential of monitoring (and controlling) aircraft attitude, which is a topic for future study.



Fig.10. View of system mounted on a model aircraft. The camera faces backwards, but the imaging system captures a frontal view.

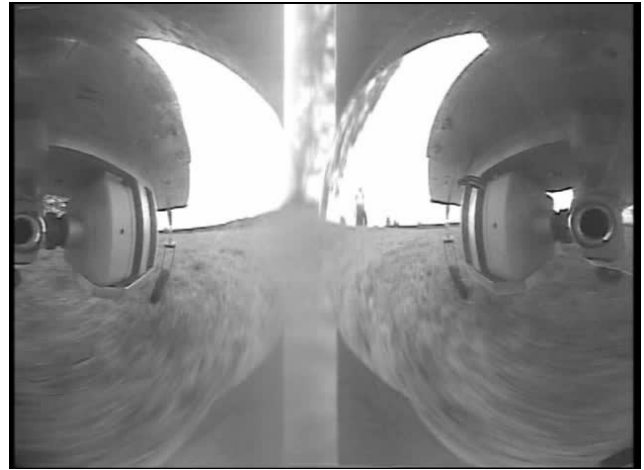


Fig. 11. Raw image of terrain as captured by left and right mirrors

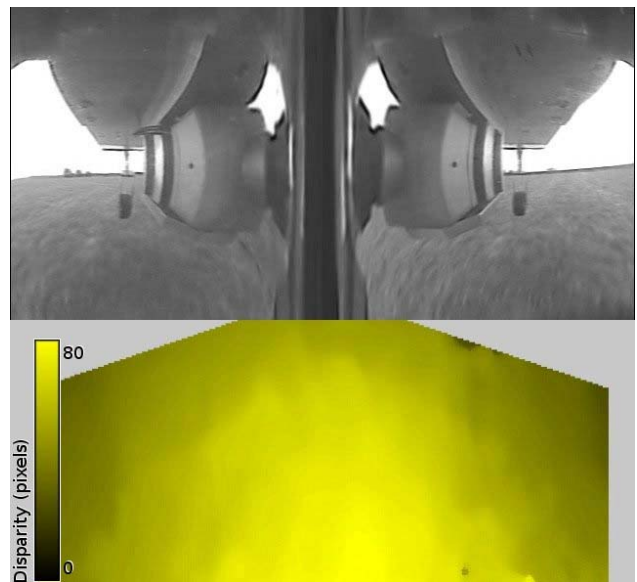


Fig. 12. Unwarped versions of the raw image in Fig. 11 (left and right, above) and disparity map (below) for level flight at a low altitude.

## 9. Conclusions

This study has described the design of a passive, near-panoramic stereo vision sensor that can be used for surveillance, measurement and control of flight height, obstacle avoidance, and landing. A video camera is used in conjunction with two specially shaped curved reflecting surfaces to achieve near-panoramic vision, and efficient computation of range through stereo. The advantage of using this visually-based method of range computation, rather than the more traditional method based on optic flow, is that information on range can continue to be obtained even when the aircraft is stationary or moving slowly.

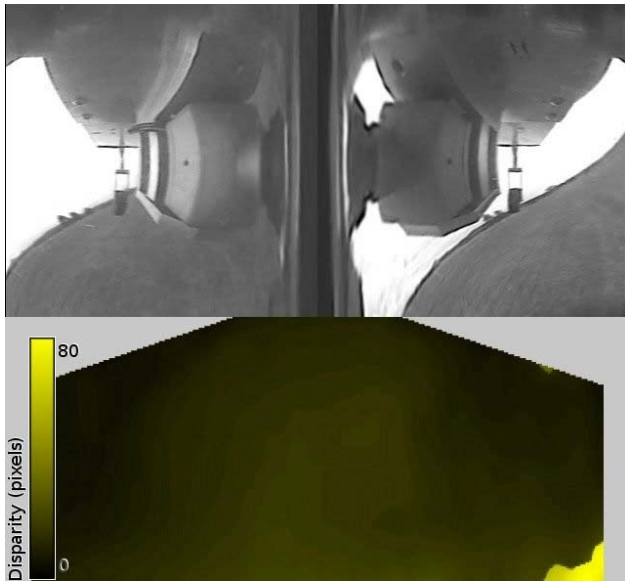


Figure 13. Unwarped images (above) and pixel disparity map (below) for higher altitude flight with positive pitch and right bank

The system also permits the acquisition of optic flow information, if desired, to assist visual guidance. Future work will explore closed-loop tests of height and attitude control, and the use of the horizon for stabilization of attitude.

## 10. Acknowledgements

This work was supported partly by the US Army Research Office MURI ARMY-W911NF041076, Technical Monitor Dr Tom Doligalski, US ONR Award N00014-04-1-0334 and the ARC Centre of Excellence Grant CE0561903.

## 11. References

- [Barrows *et al.*, 2003] G.L. Barrows, J.S. Chahl and M.V. Srinivasan. Biologically inspired visual sensing and flight control. *The Aeronautical Journal, London: The Royal Aeronautical Society* 107:1069, 159-168, 2003.
- [Chahl and Srinivasan, 1997] J.S. Chahl and M.V. Srinivasan. Reflective surfaces for panoramic imaging. *Applied Optics* 36: 8275-8285, 1997
- [Chahl and Srinivasan, 1999] J.S. Chahl, and M.V. Srinivasan. Panoramic vision system for imaging, ranging and navigation in three dimensions. *Proceedings, Field and Service Robotics Conference, Pittsburgh*, August 29-31, 127-132, 1999.
- [Fua, 1993] P. Fua. A parallel stereo algorithm that produces dense depth maps and preserves image features. *Machine Vision and Applications* 6 (1): 35-49, December 1993.
- [Hicks and Bajcsy, 2001] R.A. Hicks and R. Bajcsy. Reflective surfaces as computational sensors. *Image and Vision Computing*, 19: 773-777, 2001.
- [Nayar, 1997] S.K. Nayar. Omnidirectional video camera. *Proceedings of the 1997 DARPA Image Understanding Workshop*, May 1997.
- [Ruffier and Franceschini, 2005] F. Ruffier and N. Franceschini. Optic flow regulation: the key to aircraft automatic guidance. *Robotics and Autonomous Systems* 50:177-194, 2005.
- [Srinivasan *et al.*, 2004] M.V. Srinivasan., S.W. Zhang, J S Chahl, G Stange and M Garratt. An overview of insect inspired guidance for application in ground and airborne platforms. *Proc Inst Mech Engrs Part G*, 218: 375-388, 2004.
- [Tisse *et al.*, 2007] C-L. Tisse, O. Frank, H. Durrant-Whyte. Hemispherical depth perception for slow-flyers using coaxially aligned fisheye cameras. *Proceedings, International Symposium on Flying Insects and Robots, Monte Verita, Ascona, Switzerland*, P. 123, Aug 12-17, 2007.
- [Yagi *et al.*, 1996] Y. Yagi, W. Nishii, K. Yamazawa and M. Yachida. Stabilization for mobile robot by using omnidirectional optic flow. *Proceedings of the International Conference on Intelligent Robots and Systems*, (Institute of Electrical and Electronics Engineers, Piscataway, N.J.), 618-624, 1996.
- [Zufferey and Floreano, 2006] J.C. Zufferey and D. Floreano. Fly-inspired visual steering of an ultralight indoor aircraft. *IEEE Transactions on Robotics* 22: 137-146, 2006.